ORIGINAL ARTICLE

lajss.org
Latin American Journal of Solids and Structures

www.lajss.org

Theoretical and Experimental Study on the Performance of Steel and Concrete Multi-layer Composite Targets Against Shaped Charge Jet

Bin Chen[a], **Xudong Zu**[a*]

[a] Nanjing University of Science and Technology, School of Mechanical Engineering, Nanjing, Jiangsu, China. Email: 534442937@qq.com, zuxudong9902@njust.edu.cn

* Corresponding author

https://doi.org/10.1590/1679-7825/e8874

Abstract

To investigate the ballistic performance of a five-layer composite target plate (steelconcrete-steel-concrete-steel) under the penetration effects of a shaped charge jet, a combined approach of static explosion tests and numerical simulations was employed.The study analyzed the ability of the steel target to enhance the penetration resistance of the composite target plate and explored the reasons behind this enhancement. The research results indicate that due to the influence of reflected and transmitted waves,the steel target effectively reduces the jet's ability to create holes and penetrate the subsequent concrete target; when facing the penetration of a 200-type standard projectile, a combination of three layers of 8mm steel targets is the optimal antipenetration structure, which can enhance the protective performance of the internal concrete protective structure by 65%; After adjusting the thickness ratios of the steel target plates in the composite target plate, it was found that when only increasing the thickness of a single layer of the target plate, the first layer must be increased to 24mm or the third layer to 22mm to fully resist the penetration of the shaped charge jet;Increasing the thickness of the third layer significantly impacts the composite target plate's penetration resistance, but thickening the first layer effectively reduces the diameter of holes in subsequent concrete target plates, thereby enhancing the stability of the composite protective structure. In the overall design of composite protection,adjusting the thickness ratios between different layers can be used to address variousscenarios.

Keywords

multi-layer medium; composite target; shaped charge; numerical simulation; anti-bullet performance

Graphical Abstract

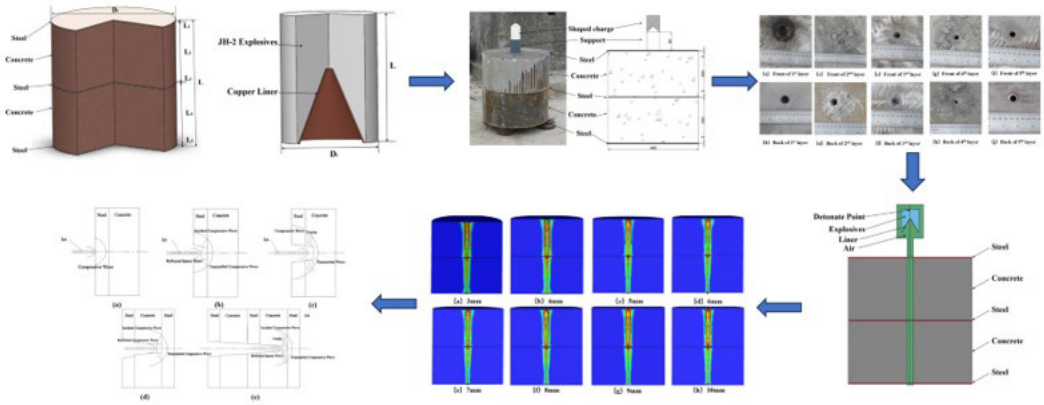

Received October 22, 2025. In revised form December 08, 2025. Accepted December 10, 2025. Available online December 12, 2025.
https://doi.org/10.1590/1679-7825/e8874

1 INTRODUCTION

On the modern battlefield, tandem warhead missiles and loitering munitions are widely employed to strike key protected targets such as command posts. For instance, cruise missiles like the U.S. Tomahawk Block IV, Germany's Taurus, and Europe's Storm Shadow utilize a precursor shaped charge to achieve axial penetration and radial hole enlargement in concrete-like protective structures. This is followed by a subsequent kinetic energy projectile that enters through the created pathway to inflict final damage on the target. Since the penetration effectiveness of the precursor shaped charge jet directly determines whether the follow-through projectile can successfully enter the target, and since ordinary concrete structures often exhibit shortcomings such as excessive hole diameter and over-penetration when resisting such jets, modern protective engineering increasingly adopts multi-medium composite structures. These are designed to degrade the hole-forming and penetration capabilities of the precursor jet, thereby enhancing the overall defensive performance against follow-through projectiles.

Extensive research has been conducted on the penetration of shaped charge jets into concrete target plates from theoretical, experimental, and numerical simulation perspectives. Early scholars devoted significant efforts to studying the resistance of single-layer concrete targets against shaped charge jet penetration. Wang Jing et al. proposed a computational model for jet penetration into concrete and validated its feasibility through experiments, providing an improved method for penetration prediction(J. Wang et al. 2008). Elshenawy et al. investigated the influence of concrete strength on penetration depth and proposed a modified Allison-Vitali equation for strength correction(Elshenawy et al. 2013). Liu Ying et al. systematically summarized the effects of parameters such as charge structure, liner type, and standoff distance on the hole formation pattern in concrete based on extensive experimental data, revealing the characteristics of hole formation capability during jet penetration into concrete(Y. Liu et al. 2025).To further enhance the penetration resistance of protective structures, most scholars have approached this by increasing concrete strength and studying the anti-penetration performance of concrete targets with different strengths. Resnyansky et al. experimentally compared the anti-jet performance of plain concrete and high-strength concrete, evaluating the protective advantages of high-strength concrete(Resnyansky et al. 2009). Zhu et al. established an axial penetration model specifically for high-strength and ultra-high-performance concrete and verified its reliability through experiments(Q. Zhu et al. 2018). Xu et al. based on large-scale shaped charge penetration tests, developed a dynamic constitutive model that describes the mechanical response of concrete under impact loading, systematically analyzing the penetration resistance of concrete with different strengths(X. Xu et al. 2017).In addition to improving the penetration resistance of the target itself, some scholars have studied the anti-penetration modes of concrete targets from the perspective of different penetration processes. Xiao et al. analyzed the impact and compression effects during supersonic penetration and established a corresponding supersonic penetration model(Q.Q. Xiao et al. 2017). Wei et al., from the perspective of combined penetration and explosion effects, analyzed the damage modes of concrete structures like airport runways under impact and blast loads(W.L. Wei et al. 2024). Zhang Xiaowei et al. investigated the changes in the anti-penetration performance of high-strength concrete targets by altering the liner material(X.W. Zhang et al. 2024). Xiao et al. also explored the enhanced damage mechanism of reactive liners against concrete targets, revealing their penetration behavior against multi-layered concrete structures(J. Xiao et al. 2018).

Regarding the anti-penetration performance of multi-medium composite targets, related research has also achieved certain progress. Kang Yanlong et al. compared the penetration effects of copper, mild steel, and titanium alloy liners into multi-layer medium targets and analyzed the propagation characteristics of stress waves during penetration(Y.L. Kang et al. 2012). Xiao Qiangqiang et al. comprehensively utilized theoretical, simulation, and experimental methods to study the penetration behavior of shaped charges into typical soil-concrete composite media(Q.Q. Xiao et al. 2012). Xiao et al., from the perspective of detonation wave propagation at medium interfaces, proposed an analytical model for the penetration of shaped charge jets into soil-concrete double-layer targets(Q.Q. Xiao et al. 2017). Zhang et al. employed a coupled SPH-FEM numerical method to simulate the damage modes of jets penetrating steel-SPS composite targets and validated the rationality of the simulation model(Z. Zhang et al. 2016).Beyond combining different materials with concrete, most scholars tend to favor composite armor composed of ceramics and various fiber materials when designing composite targets. Lu Wencheng et al. designed SiC ceramic-fiber reinforced resin matrix composite armor, tested the anti-penetration performance with different thickness ratios, and structurally optimized the ceramic composite target(W.C. Lu et al. 2024). Liu et al. investigated the influence of fiber hybridization and stacking sequence in composite armor on its protective performance and designed a novel structured composite armor to enhance the target's anti-penetration capability(Z. Liu et al. 2025). Acat et al. studied the variation in the ballistic performance of ceramic/metal composite armor by changing the strength and thickness of the adhesive layer(Acat et al. 2025).However, existing research predominantly focuses on

double-layer composite targets or high-strength concrete targets. Systematic studies on the resistance of triple-layer or multi-layer composite structures against shaped charge jet penetration remain relatively scarce.

Research on the propagation process of stress waves in layered media has been relatively comprehensive by relevant scholars.Since the 20th century, theoretical research on stress wave propagation in layered media has been extensively conducted. In the 1950s, Haskell first analyzed the dispersion characteristics of surface waves in layered media(Haskell et al. 1953). In the 1990s, Lamb systematically addressed the propagation of vibrations in isotropic elastic half-spaces, expanding the theories of two- and three-dimensional wave fields(Lamb et al. 1904). In 1992, Li Xibing et al. applied boundary conditions of rock mass structural planes to establish the reflection-transmission relationships for explosive stress waves obliquely incident on weak structural planes(X.B.Li et al. 1992). In 1995, Wang Mingyang and Qian Qihu combined geological structural features to numerically analyze the propagation of stress waves in fracture zones, noting that within specific ranges of Poisson's ratio and friction angle, higher degrees of fault fragmentation lead to faster energy attenuation(M.Y.Wang et al. 1995). In 2014, Lu Dawei et al., focusing on drill-and-blast construction, conducted an in-depth study on the propagation paths and energy attenuation patterns of explosive stress waves(D.W. Lu et al. 2014). However, studies on the propagation process of detonation waves in continuous media such as composite target plates remain to be further explored.

Based on comprehensive research findings, common target plate materials for countering shaped charge jets are concrete and armored steel. Due to the higher impedance of armored steel compared to concrete, stacking armored steel above the concrete layer provides superior protective effectiveness. This study proposes a multi-layer protective structure composed of three steel plates and two concrete target layers, and static explosion tests were conducted. The target employs armored steel and C40 concrete, adopting a five-layer steel-concrete-steel-concrete-steel sandwich configuration. Based on the static explosion test results, a comparative analysis was carried out with the penetration depth and hole diameter in plain concrete targets penetrated by jets. It was found that the steel plates significantly influence the enhancement of the composite target's anti-penetration performance. Subsequently, by establishing a numerical simulation model and analyzing the dynamic response of the concrete targets within the composite structure, the study revealed the improvement effect of the steel plates on the concrete's anti-penetration performance. Finally, from the perspective of structural matching, the thickness of each steel layer was analyzed and optimized to explore the optimal configuration for resisting shaped charge penetration. Through the analysis of the influence of the multi-layer protective structure on the hole formation and penetration depth against shaped charge jets, this research can provide a basis for the design of multi-medium protective structures, contributing to the further enhancement of the ballistic resistance and protective capacity of both civil and military protective engineering.

2 Experiments

2.1 Test Projectile and Target Plate

The projectile selected for the test was a Type 200 reference projectile. It featured a charge diameter of 56 mm and was equipped with a conical liner made of copper with a thickness of 1 mm. The main charge was pressed from JH-2 explosive, with a charge height of 73 mm. The shaped charge used is shown in Figure 1.

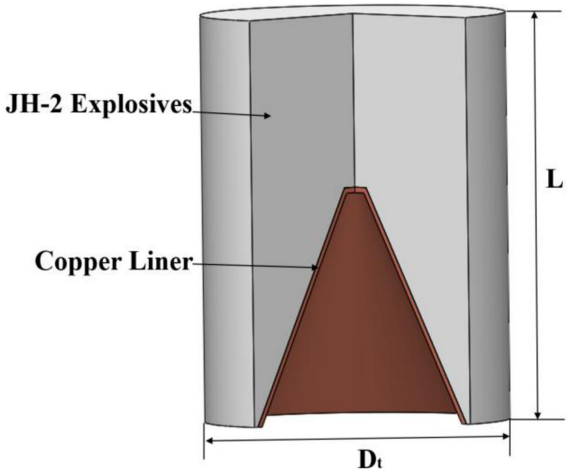

Figure 1. Structure of the Test Shaped Charge.

The concrete target plates used in the experiment were cast plain concrete plates with dimensions of ϕ400 mm × 200 mm. The materials selected included 42.5-grade cement, crushed stone with a particle size range of 5–25 mm, and medium-grade sand. The surface of the target plate was smooth and flat, enabling it to closely adhere to the steel target, thereby minimizing the influence of interstitial air on the penetration performance of the jet. The density of the concrete is 2430 kg/m^3, and the compressive strength of the concrete target plate is 40 MPa. The homogeneous armor steel target used is a thin plate with dimensions of ϕ400 mm × 3 mm. The density of the armor steel is 7800 kg/m^3, the tensile strength is 1280 MPa, and the hardness is 425 HB. Table 1 provides the mechanical performance parameters of each target plate.

Table 1 Mechanical properties of concrete and armored steel used in the test

Materials	Density (kg/m^3)	Poisson ratio	Modulus of elasticity (Gpa)	Yield strength(Mpa)
Concrete	2430	0.15	32.5	26.8
Steel	7800	0.29	205	792

Arrange and stack the prepared target plates in the specified order (steel target, concrete target, steel target, concrete target, steel target) as shown in Figure 2. In the figure, D_t = 400 mm, L = 409 mm, and L_1–L_5 represent the thicknesses of each layer, which are 3 mm, 200 mm, 3 mm, 200 mm, and 3 mm, respectively. When arranging the target plates, place steel ingots at the bottom of the target plates to keep them level. To prevent lateral pressure, no bonding is performed between the layers of target plates.

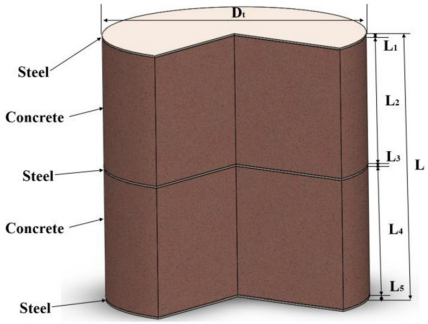

Figure 2. Schematic diagram of a five-layer composite target.

2.2 Design of the Static Blast Experiments

The experiments were designed with shaped charge jets penetrating both plain concrete and composite targets, creating a comparative setup. An air standoff of 80 mm was selected. The arrangement of test specimens in the experimental field is shown in Figure 3, with the shaped charge, standoff tube, composite target, and steel block positioned sequentially from top to bottom. The steel block was placed beneath the composite target to ensure the target remained level, thereby guaranteeing stable projectile alignment and vertical penetration. After the test, the damage conditions on the front and rear surfaces of each layer in the composite target could be observed.

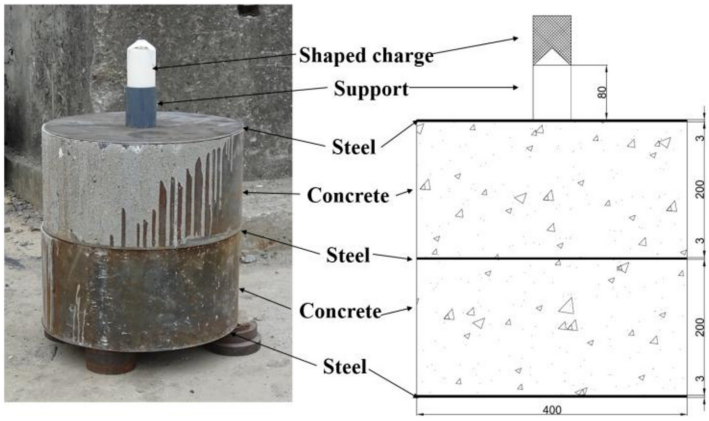

Figure 3. Static Blast Experiment Layout Diagram.

3 Experimental results and analysis

3.1 Jet penetration test results on plain concrete

The damage condition of the concrete targets after the test is shown in Figure 4. As can be observed from the figure, significant large-area spalling occurred on the surface of the plain concrete target, with radial cracks extending from the edges of the spalling crater. The diameter of the spalling zone is approximately 300 mm. The 400 mm thick plain concrete target was completely penetrated by the jet, while the jet also created a relatively large entry hole on the target surface, with a diameter of about 28 mm.

Figure 4. Jet penetration experiment results on plain concrete.

3.2 First experiment results of jet penetration composite target plate

After the experiment, the target plates were recovered, and it was found that all layers of the composite target plates had been penetrated. The first layer of steel target was directly blown away due to the large shock wave, and the target plate was penetrated, forming a large opening; the second layer of concrete target cracked significantly and broke directly; the third layer of steel target was penetrated but had a smaller opening; the fourth layer of concrete target formed a small crater on the front side and a larger crater on the back side, with the opening further reduced; the fifth layer of steel target was penetrated, with the opening further reduced. The opening conditions of each layer of the composite target plate after the first experiment are shown in Figure 5, and the penetration results are shown in Table 2.

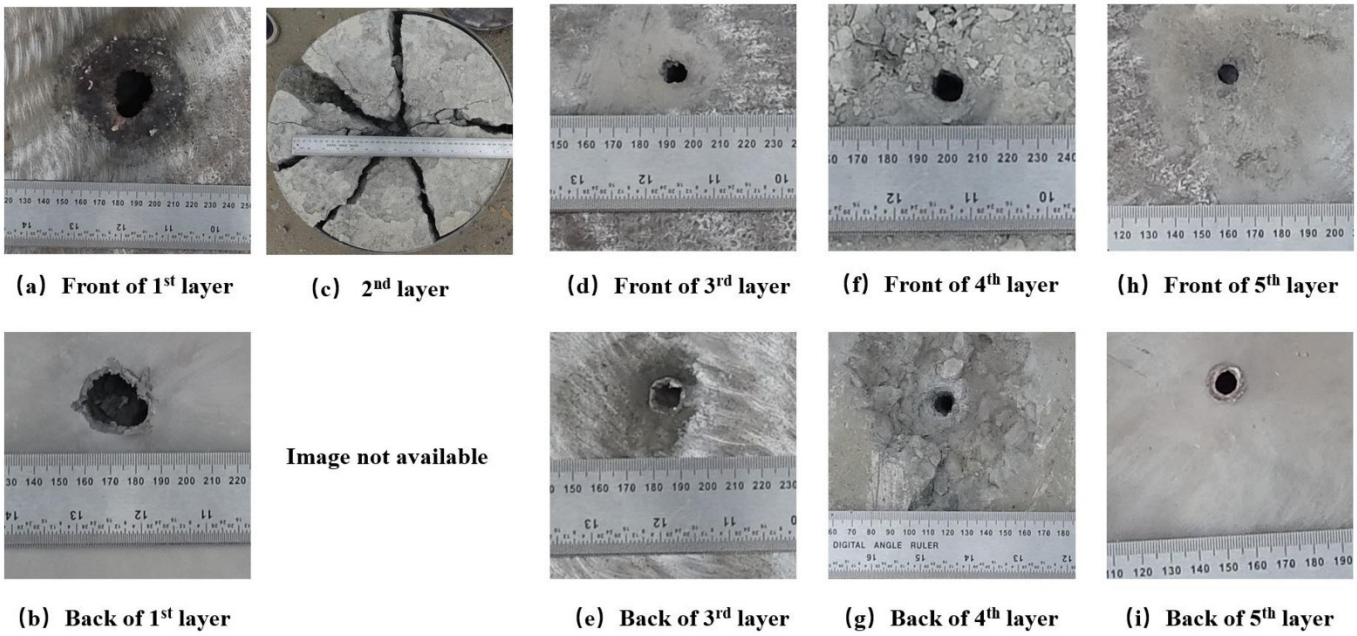

Figure 5. Damage to the first experiment target plate.

Table 2 First shot penetration experiment results

Target plate number	Materials	Thickness(mm)	Manhole(mm)	Exit hole(mm)
1	Steel	3	19	19
2	Concrete	200	cracked	cracked
3	Steel	3	10	10
4	Concrete	200	10	8
5	Steel	3	8	7

3.3 Second experiment results of jet penetration composite target plate

Due to the shattering of the second concrete layer in the composite target from the first test, which prevented detailed measurement and analysis, a supplementary comparative test was conducted.After the second test, it was found that all layers of the composite target were penetrated. The first steel layer was dislodged by the blast wave, with the target being penetrated and forming a large crater. The second concrete layer was penetrated with a large crater; its front face exhibited significant spalling, while the spalling on its rear face was minimal. The third steel layer was penetrated but with a smaller crater. The fourth concrete layer was penetrated with a relatively small crater; its rear face showed significant spalling, while the spalling on its front face was minor. The fifth steel layer was penetrated, with the crater size further reduced.The crater conditions in each layer of the composite target after the second test are shown in Figure 6, and the penetration results are summarized in Table 3.

Table 3 Second shot penetration experiment results

Target plate number	Materials	Thickness(mm)	Manhole(mm)	Exit hole(mm)
1	Steel	3	19	18
2	Concrete	200	18	11
3	Steel	3	10	10
4	Concrete	200	9	8
5	Steel	3	8	7

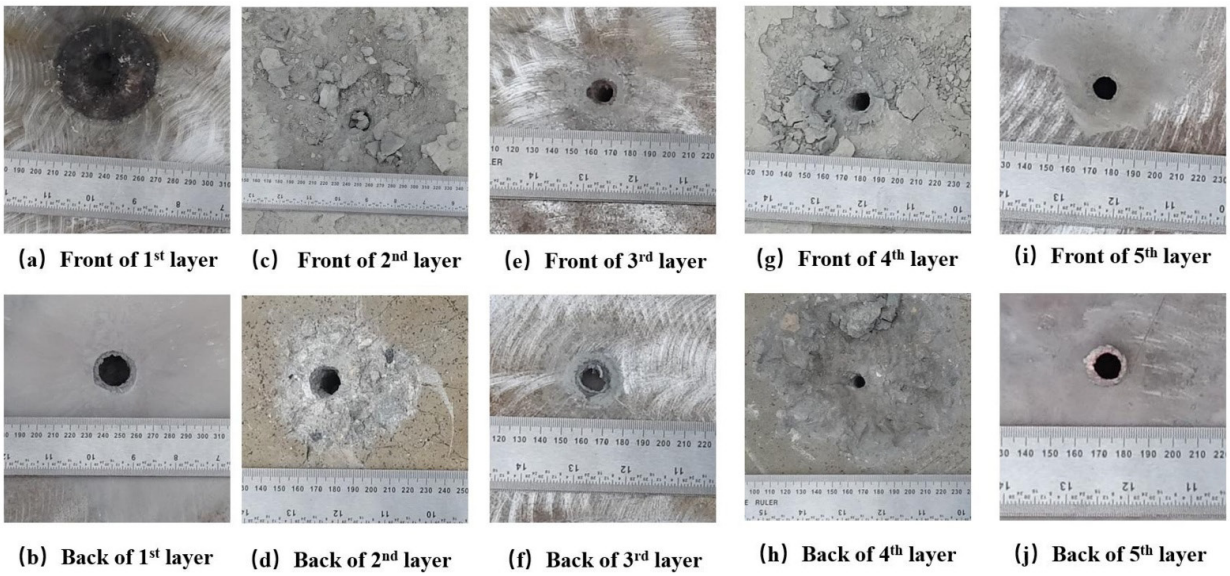

Figure 6. Damage to the second experiment target plate.

3.3 Results Analysis

The results of the two experiments revealed that the composite target failed to successfully withstand the shaped charge jet. Due to the protective effect of the first layer of steel target, the diameter of the holes and the collapse zone of the second layer of concrete target were significantly reduced. Compared to the collapse zone diameter of 300 mm

produced during the excavation phase when the shaped charge directly penetrated the plain concrete target, the diameter of the fragmentation zone on the second layer of concrete target plate was only 105 mm, reducing the fragmentation zone area by 65%. The hole diameter decreased from approximately 28 mm (0.5 times the charge diameter) to 17 mm, reducing the penetrator's hole-making capability by 39%. Additionally, significant crack propagation was observed on the back of the first layer of steel target, resulting in some layer-wise damage. The protective effect of the third layer of steel target resulted in a very small collapse zone formed between the back of the second layer of concrete target and the front of the fourth layer of concrete target plate. Similarly, due to the protective effect of the fifth layer of steel target, the area of the collapse zone on the back of the fourth layer of concrete target plate was also reduced.

To more intuitively observe the protective effect of the steel layer on the subsequent concrete target, a comparison was made between the crater diameter formed by the jet directly penetrating the plain concrete target and that formed in the upper concrete layer of the composite target protected by the steel layer. It was found that, under the protective influence of the steel layer, the jet's ability to form craters and penetrate the subsequent concrete target was significantly reduced. A comparison of the damage between the upper concrete layer in the composite target and the plain concrete target directly penetrated by the jet is shown in Figure 7.

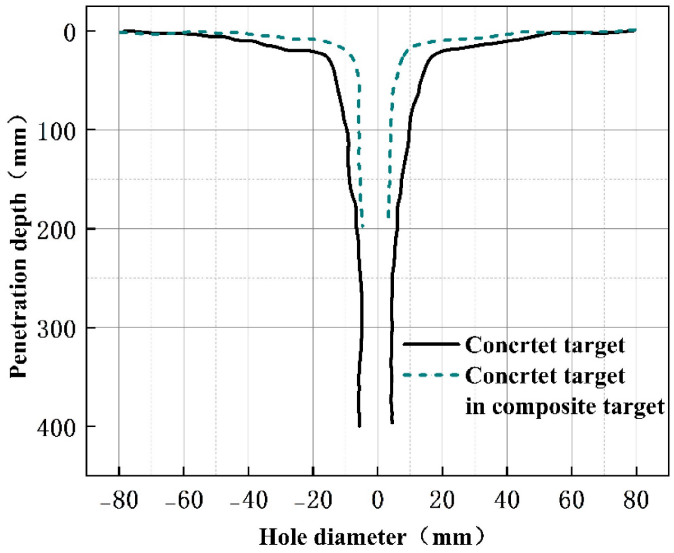

Figure 7. Comparison of concrete target damage.

4 Numerical simulation analysis

4.1 Material model establishment

To better study the protective performance of composite target plates and explore the optimal structural design, three-dimensional finite element simulation was performed using LS-DYNA simulation software. Considering the symmetry of the projectile and target plate, only a quarter of the model was constructed to reduce computational power. The mainstream computational method for studying jet penetration of target plates is the ALE algorithm, so an Eulerian mesh was used to establish the model of the 200-type reference projectile. The five-layer composite target plate model was designed using a gradually sparse Lagrange mesh with a dense center and sparse periphery. Finally, the fluid-structure interaction keyword was used to simulate the penetration of the jet into the target plate.

The propellant in the projectile body uses the MAT-HIGH-EXPLOSIVE-BURN model, described by the JWL state equation. The material parameters are shown in Table 4(Z.H. Du et al. 2017), where ρ is the initial density of the explosive, D is the detonation velocity of the explosive, E is the internal energy per unit volume of the explosive, and A, B, R_1, R_2, and ω are material constants.

Table 4 JH-2 Material Parameters

ρ/(g/cm³)	D/(km/s)	A/GPa	B/GPa
1.713	7.98	524.2	7.768
R_1	R_2	ω	E/GPa
4.2	1.1	0.34	8.45

The copper liner in the projectile body uses the Johnson-Cook model, with material parameters as shown in Table 5(Z.H. Du et al. 2017), where ρ is the material density, G is the shear modulus, T_m is the softening temperature of the material, and A, B, C, n, and m are material constants.

Table 5 Material parameters of copper liner

ρ/(g/cm³)	G/GPa	A/GPa	B/GPa
8.96	47.7	350	275
C	n	m	T_m
0.36	0.022	1.09	1356

For the ALE method, it is also necessary to establish an air model for the jet flight range and apply pressure outflow boundary conditions at the boundary points to avoid pressure reflection at the boundary. The air uses the NULL model, and the material parameters are shown in Table 6(Y.H. Gao et al. 2013).

Table 6 Air material parameters

ρ/(g/cm³)	C/(m/s)	E/(kJ/ cm³)	V/ cm³
81.26×10^{-3}	394	0	1

The primary failure mode of concrete in composite target plates is compressive failure during the jet penetration process. Therefore, the RHT model is used to describe the failure process of concrete, with material parameters as shown in Table 7(C. Su et al. 2024). For steel targets, the Johnson-Cook model is employed, with material parameters as shown in Table 8(W.Y. Wen et al. 2001).

Table 7 Concrete material parameters

$\rho_0 / g\bullet cm^{-3}$	P_{el} / Mpa	P_{comp} / MPa	N	α_0	A_1 / GPa
2.32	23.3	600	3.0	1.1884	35.27
f_c / MPa	f_t^*	f_s^*	G / GPa	A	n
40	0.1	0.18	16.7	1.6	0.61
Q_0	B	β_c	β_t	$\dot{\varepsilon}_0^c / ms^{-1}$	A_2 / GPa
0.6805	0.0105	0.032	0.036	3.0E-8	39.58
A_3 / GPa	B_0	B_1	T_1 / GPa	T_2 / GPa	$\dot{\varepsilon}_0^t / ms^{-1}$
9.04	1.22	1.22	0.05	0	3.0E-9
$\dot{\varepsilon}^c / ms^{-1}$	$\dot{\varepsilon}^t / ms^{-1}$	g_c^*	g_t^*	ξ	ε_p^m
3.0E22	3.0E22	0.53	0.7	0.5	0.01

Table 8 Armored steel material parameters

ρ/(g/cm³)	G/GPa	A/GPa	B/GPa
7.82	77	507	320
C	n	m	T_m
0.064	0.028	1.06	1793

4.2 Numerical simulation results and comparison

For the numerical simulation model of the design, by studying the penetration process of the jet on the composite target plate, it can be observed that the penetration time of the jet on the composite target plate is extremely short, with penetration completed within 270 μs. Additionally, the jet's hole-making capability decreases as the penetration depth increases, consistent with the experimental results. The damage condition of the composite target plate is shown in Figure 8. By comparing the hole diameters of each layer of the target plate between simulation and experiment, it can be seen that the simulation results are in good agreement with the experiment results, with a maximum error of 7.78%. The comparison results are shown in Figure 9.

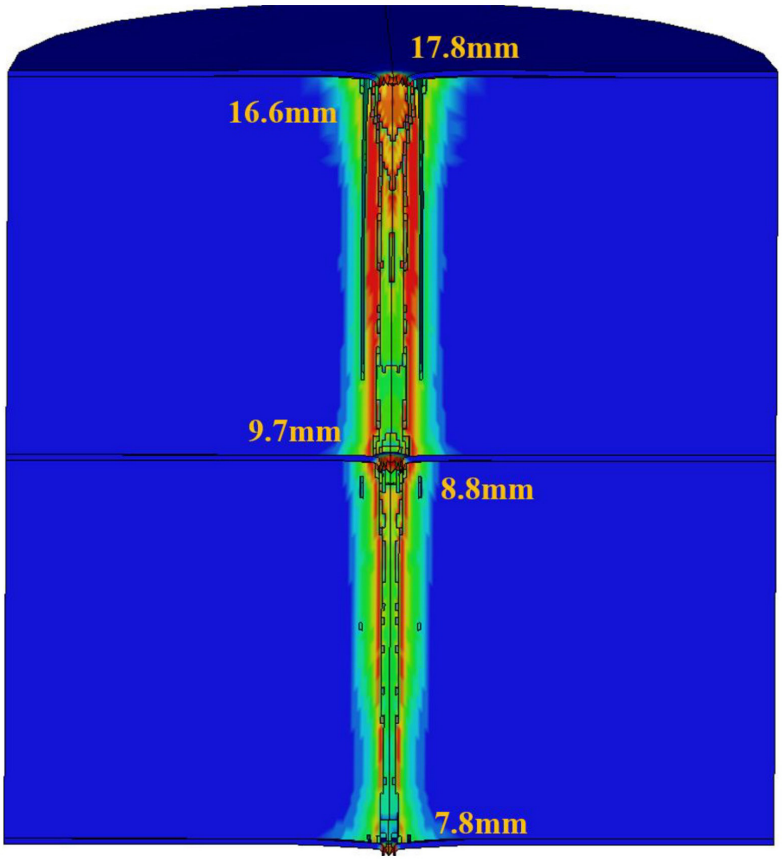

Figure 8. Damage to composite target plates.

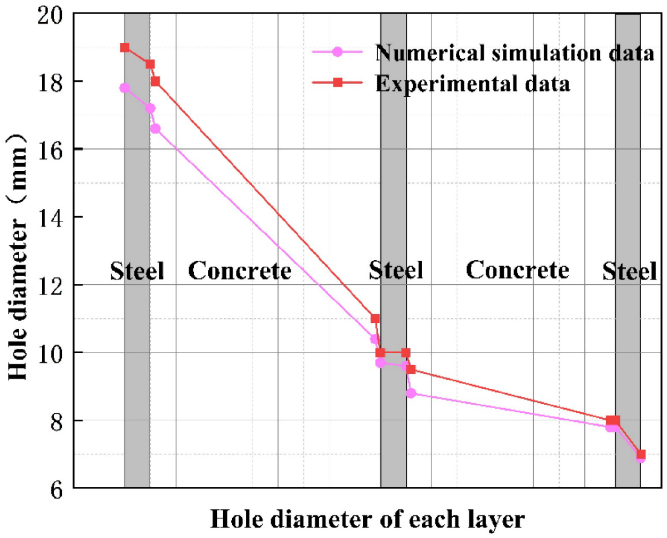

Figure 9. Hole diameter comparison chart.

To better evaluate the protective enhancement provided by the steel layer to the concrete target and to optimize the subsequent structure, a numerical simulation of the shaped charge jet penetrating plain concrete was conducted to determine the ultimate penetration depth. Consistent with the experimental results, the shaped charge jet caused significantly more damage to the concrete target in the absence of steel plates. Under the same conditions, the jet created a crater with a diameter of 28.7 mm on the surface of the C40 plain concrete target and achieved a maximum penetration depth of 660 mm. The damage condition of the plain concrete target is shown in Figure 10.The entire penetration process lasted 800 μs, during which the jet velocity decreased relatively gradually. In contrast, the jet exhibited a more pronounced velocity reduction over the 270 μs penetration process into the composite target. The velocity variations of the jet during penetration into the different targets are shown in Figure 11.

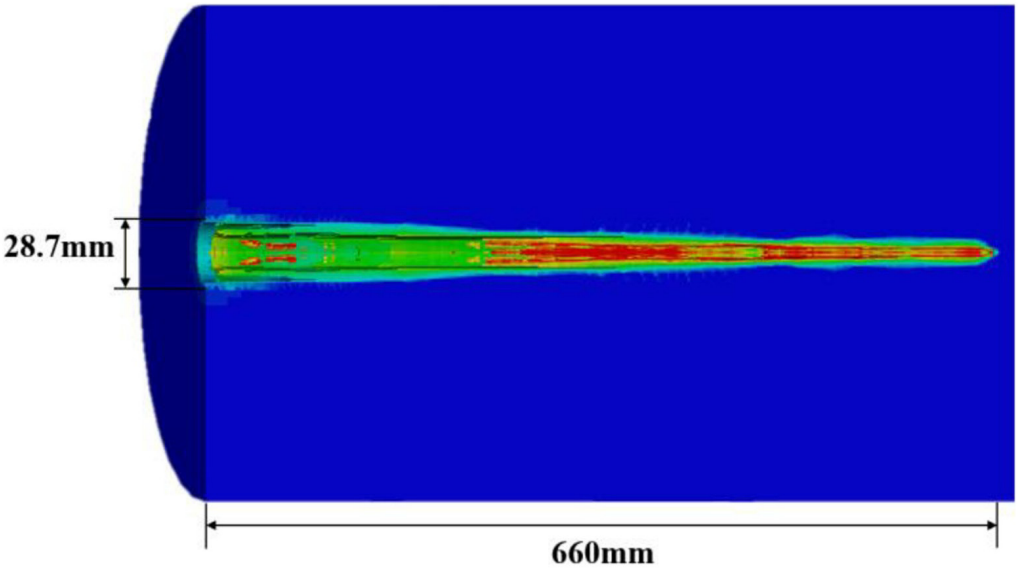

Figure 10. Damage to plain concrete.

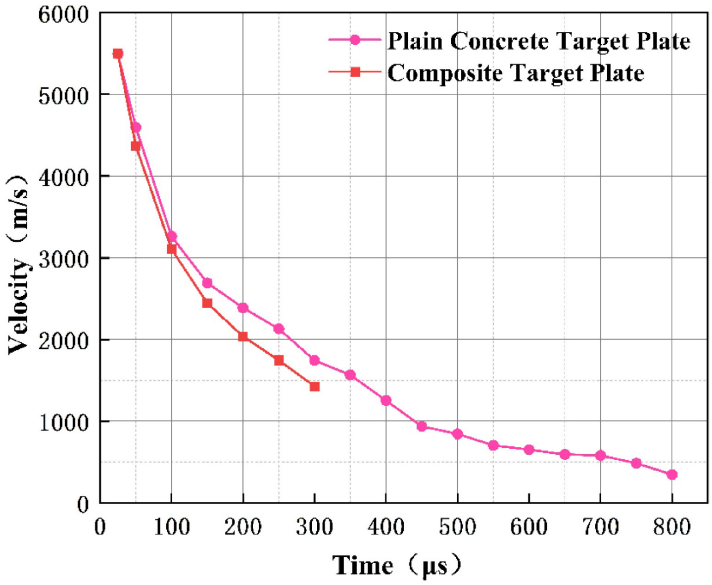

Figure 11. Velocity changes when a jet penetrates different target plate.

To investigate the effect of steel target thickness on the anti-penetration performance of composite target plates and optimize their structure, multiple numerical simulation models were designed with three layers of steel targets, each increasing in thickness by 1 mm in a stepwise manner. The study found that when all three layers of steel targets were increased to 8 mm, they could just withstand the penetration of a shaped charge jet. To contrast with the scenario where the shaped charge jet penetrates the target plate and to ensure the rigor of the simulation, additional simulation

scenarios with steel targets of 9 mm and 10 mm thickness were added. The damage conditions of the composite target plates in each scenario are shown in Figure 12. Combining the simulation results with the findings of Hou Junchao[14] et al. , it was found that in the designed composite target plate, the 24 mm thick steel target and the 260 mm thick plain concrete exhibit identical penetration resistance performance in terms of resisting jet penetration depth. Since the difference in the entry and exit holes of the fourth layer of concrete target under the protective effect of the two layers of steel targets is only about 1mm, only the hole diameter changes of the two layers of concrete targets were analyzed. By comparing different findings, it was found that as the thickness of the steel target increases, the jet's ability to create holes in the concrete target also decreases. The changes in the hole diameter of the concrete target when the thickness of the steel target is altered are shown in Figure 13.

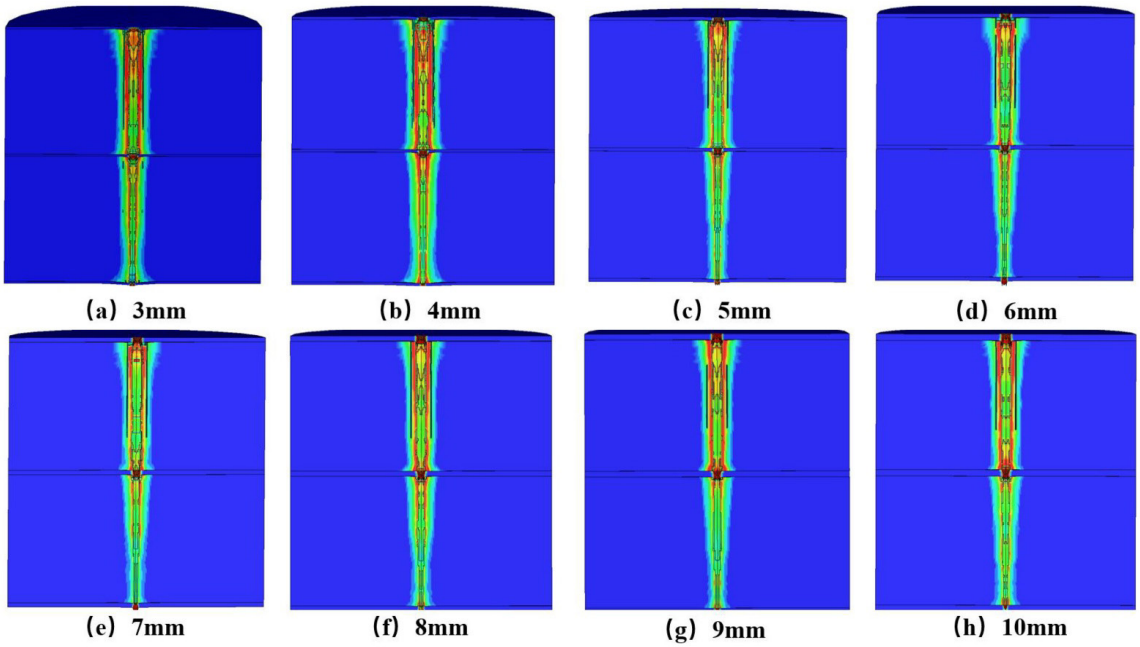

Figure 12. Damage to composite target plates under steel targets of different thicknesses.

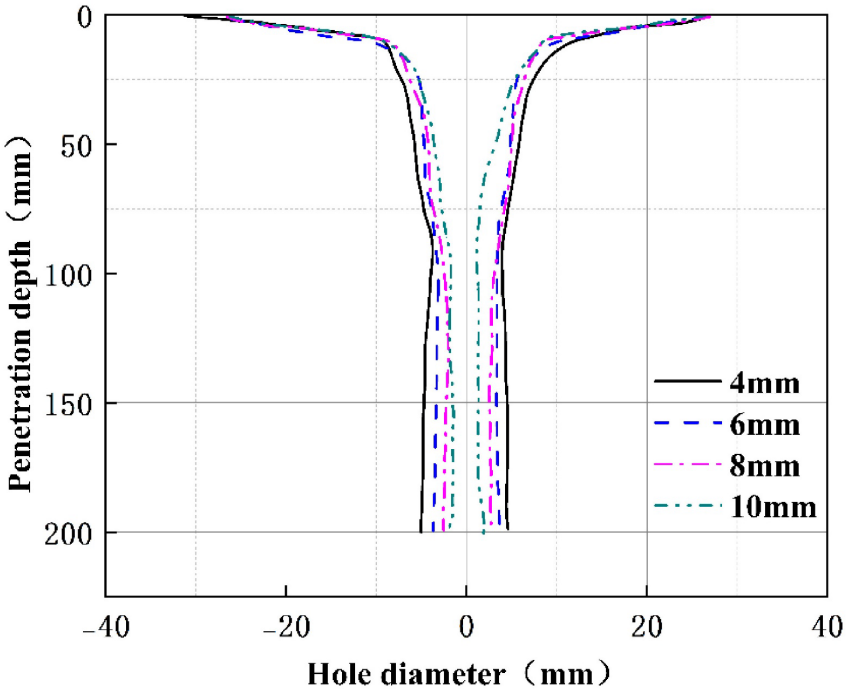

Figure 13. Concrete target hole diameter change chart.

By observing the penetration process of numerical simulations with different group numbers, it was found that the jet broke apart when penetrating the fourth layer of concrete target. The broken jet head still had a high velocity and could penetrate the concrete target plate. Since the jet head had already undergone multiple fractures by the time it penetrated the fifth layer of the steel target, its penetration capability was significantly reduced, resulting in the consumption of more energy to complete the penetration. The remaining velocity of the jet when penetrating the composite target plate is shown in Table 9 . When the jet head reaches the fifth layer of the steel target with a large number of fractures and low velocity, it cannot penetrate the fifth layer of the target plate. The velocity changes when the jet cannot penetrate the composite target plate are shown in Figure 14.

Table 9 Jet residual velocity

Steel plate thickness(mm)	Completion time of penetration(μs)	Residual velocity(m/s)
3	270	1429
4	280	1402
5	295	1326
6	305	1238
7	320	1177

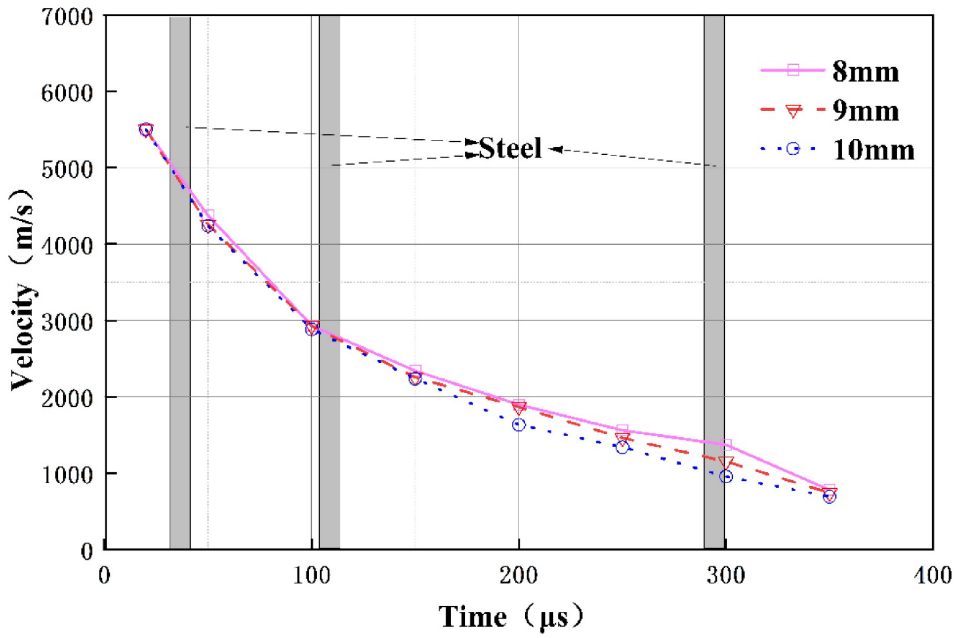

Figure 14. Changes in jet head velocity when not penetrated.

5 Dynamic response of composite target plates during penetration

Through static blast experiments and multiple numerical simulations, it was found that the steel target in the composite target plate can greatly reduce the ability of the jet to open holes and penetrate the subsequent concrete target. To further investigate the reasons why the steel target can improve the anti-penetration performance of the composite target plate, theoretical analysis and verification were conducted from the aspects of target plate damage patterns, the influence of interface effects, and the optimization of the composite target plate structure.

5.1 Damage patterns of each layer of target plates in composite target plates

The penetration process of a focused jet on a steel-concrete composite target can be roughly divided into five stages. In the first stage, the jet collides with the first layer of the steel target, generating stress waves within the material, primarily compression waves, as shown in Figure 15(a). At this point, the peak stress generated by the incident wave is approximately 25 GPa, causing the front surface of the steel target to melt and form a crater.

The jet penetrates the first layer of steel target and begins to penetrate the second layer of concrete target, entering the second penetration stage. Due to the different wave impedances of steel and concrete, when the stress waves generated by the focused jet penetrating the steel target propagate to the concrete interface, the incident waves undergo reflection and transmission at the interface, producing longitudinal transmitted waves and reflected waves. Since the wave impedance of steel is greater than that of concrete, the incident compression waves reflect at the interface and transform into rarefaction waves, forming reflected tensile waves. The reflection coefficient R and transmission coefficient T at the steel-concrete interface are

$$\begin{cases} R = \dfrac{Z_s - Z_c}{Z_s + Z_c} \\ T = \dfrac{2Z_s}{Z_s + Z_c} \end{cases} \tag{1}$$

In the equation, Z_s is the wave impedance of the armored steel, and Z_c is the wave impedance of the concrete. At this point, the reflection coefficient is 0.6, and a large amount of compression waves are reflected as tensile waves back to the steel target, causing the steel plate to separate from the concrete. At the same time, the back of the steel target is damaged, producing cracks and layer separation damage, as shown in Figure 15(b).

The transmitted wave then enters the concrete, creating a high-pressure zone near the interface. Due to energy loss caused by transmission, the compressive stress of the transmitted wave on the concrete target is approximately 20 GPa. At this point, radial cracks form in the concrete target and propagate radially outward. The front surface of the concrete target fractures until the cracks are stopped by the constraint of the third steel target. As the jet continues to penetrate, the fragmentation zone also continues to expand, as shown in Figure 15(c). The transmitted wave propagates through the concrete target plate as a spherical wave, with the wavefront stress decreasing with increasing propagation distance. The transmission coefficient of the concrete target is approximately 0.8, resulting in a stress of around 8 GPa when the transmitted wave reaches the back of the concrete target. This leads to differences in the effect of the jet at different penetration depths. The intensity of the transmitted wave is highest at the steel-concrete interface, thus causing the most significant disturbance to the jet penetration process.

The transmitted wave continues to propagate within the concrete. When it encounters the subsequent steel target interface, it undergoes reflection and transmission again, entering the third penetration stage. Since the wave impedance of steel is greater than that of concrete, the reflected wave is a compression wave, placing the back surface of the concrete target under triaxial compressive stress. This inhibits microcrack propagation, preventing spalling, as shown in Figure 15(d). At this point, the compressional wave stress entering the third steel target layer is approximately 4 GPa. The steel target is supported by the concrete target, resulting in relatively uniform stress distribution, thus no cracks form. Only a depression forms at the entry hole on the front surface of the target plate, and a slight bulge forms at the exit hole on the back surface.

When the stress wave propagated to the fourth concrete layer, marking the fourth stage of penetration, significant energy attenuation occurred due to spherical wave decay and multiple interface reflections. The reflection and transmission patterns of the stress wave in this stage were similar to those in Stage 2. However, by the time the compressive wave reached the rear face of the concrete target, its stress had diminished to only 0.5 GPa. In contrast to Stage 2, the failure mode of the fourth concrete layer was dominated by shear-compression, with cracks forming a conjugate network along the planes of maximum shear stress.

The final stress wave propagates to the fifth layer of steel target, marking the onset of the fifth stage of penetration. The back surface of the fifth layer of steel target is an air interface, where the compression wave undergoes near-total reflection at the steel-air interface, generating a reflected tensile wave that propagates back to the back surface of the fourth layer of concrete target. This places the concrete back surface under uniaxial dynamic tensile stress, resulting in large-scale spalling, as shown in Figure 15(e). At this point, the stress propagating to the steel target is very small, below the material's yield strength, and the target plate is only perforated, with no obvious cracks or other forms of damage.

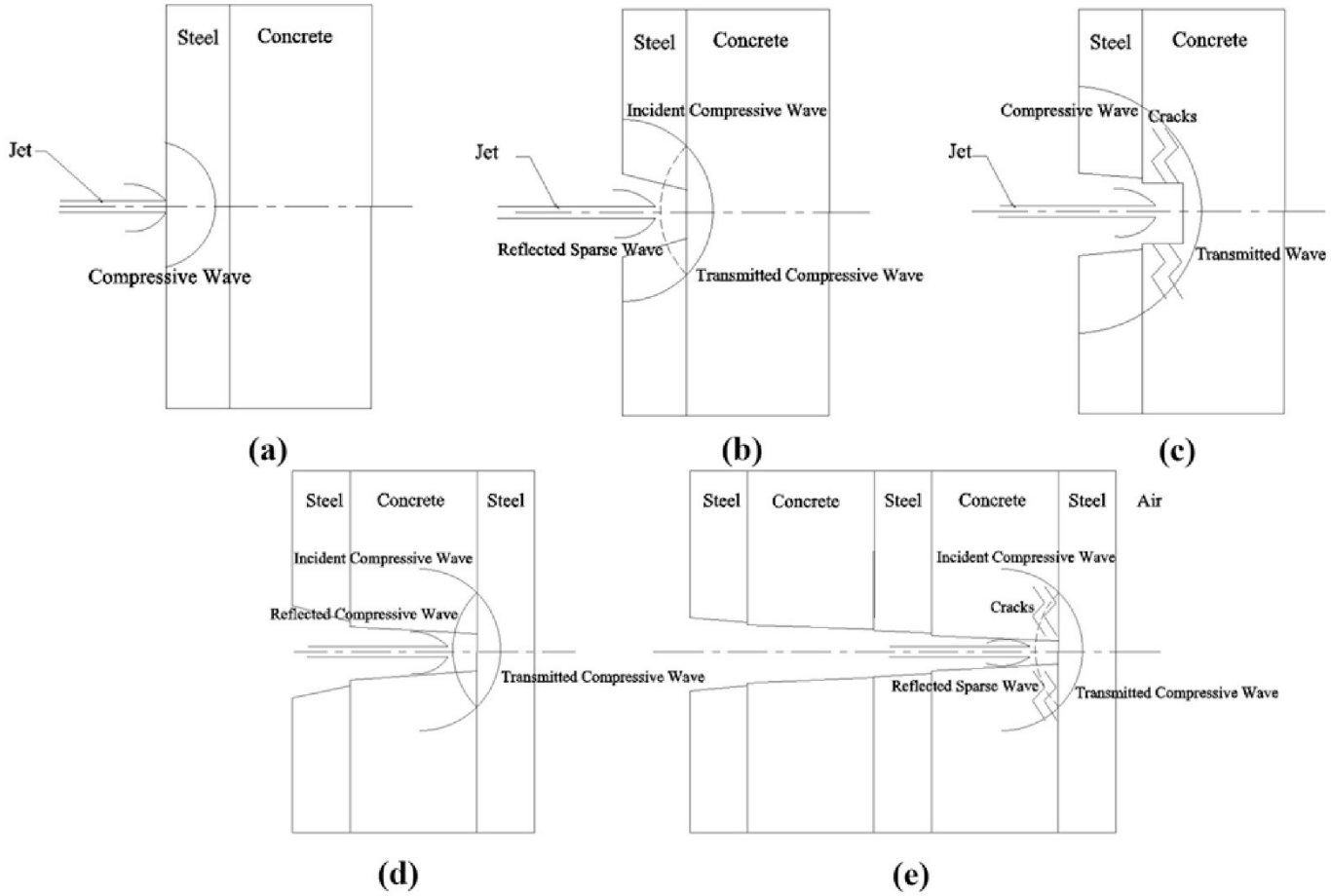

Figure 15. Penetration process of jets on composite target plates.

5.2 The Effect of Interface Effects on Jet Penetration of Composite Target Plates

Analysis of the damage patterns of the five-stage target plates reveals that the process by which the jet penetrates from the steel target to the concrete target is relatively complex and warrants further analysis. When the stress wave reaches the steel-concrete interface, it generates reflected and transmitted waves, which propagate toward the steel target and concrete target, respectively. Based on the theory of wave reflection and transmission, the relationships between the pressure and particle velocity of the reflected and transmitted waves and the incident wave can be derived as follows:

$$\begin{cases} \dfrac{p_R}{p_I} = \dfrac{\rho_C C_C - \rho_S C_S}{\rho_C C_C + \rho_S C_S} \\ \dfrac{v_R}{v_I} = \dfrac{\rho_S C_S - \rho_C C_C}{\rho_C C_C + \rho_S C_S} \\ \dfrac{p_T}{p_I} = \dfrac{2\rho_C C_C}{\rho_C C_C + \rho_S C_S} \\ \dfrac{v_T}{v_I} = \dfrac{2\rho_S C_S}{\rho_C C_C + \rho_S C_S} \end{cases} \tag{2}$$

In the equation, ρ_C and C_C represent the density and sound velocity of concrete, ρ_S and C_S represent the density and sound velocity of steel, p_R and v_R represent the pressure and particle velocity of the reflected wave, p_T and v_T represent the pressure and particle velocity of the transmitted wave, p_I and v_I represent the pressure

and particle velocity of the incident wave. Since the density and sound velocity of steel are both greater than those of concrete, the pressure and velocity of the reflected tensile wave formed at the steel-concrete interface are greater than those of the transmitted compressional wave, thereby reducing the penetration capability of the jet on the subsequent concrete target.

Due to the relatively thin thickness of the steel target plate in the composite target plate design, the jet maintains a high velocity when penetrating the steel plate and invading the concrete target plate. Therefore, the jet undergoes supersonic penetration in the steel target plate and transitions from supersonic to subsonic penetration in the concrete.

When the compression wave propagates to the steel-concrete interface, the shock wave reflects at the interface. The reflected wave begins to propagate in the steel target, while the transmitted wave propagates in the concrete target. From the conservation of mass and momentum, the changes in the state parameters of the concrete material can be determined. Additionally, from the continuity relation at the interface, it can be concluded that the pressure and particle velocity in the steel target and concrete target at the interface are equal(Q.Q.Xiao et al. 2016). Therefore, by establishing a coordinate system with its origin on the interface axis, and using the state parameters of the concrete material at penetration depth P and the Bernoulli equation, the control equation for the concrete component when the shaped charge jet penetrates the composite target plate can be derived as

$$\frac{1}{2}\rho_j\left(v_j-u\right)^2=\frac{1}{2}\rho_{cTP}\left(u-v_{cTP}\right)^2+\rho_{cTP}v_{cTP}\left(v_{cTP}-u_{sTP}\right)+R_{hc} \tag{3}$$

The control equation for the radial hole enlargement process is

$$\frac{1}{2}\rho_{c0}u_c^2+\frac{D_0^2}{D_c^2}\rho_{cTP}v_{cTP}\left(v_{cTP}-u_{sTP}\right)+R_{hc}=\frac{D_0^2}{2D_c^2}\rho_j\left(v_j-u\right) \tag{4}$$

In the equation, ρ and v represent density and particle velocity, respectively; u is the jet penetration velocity; D is the pore diameter; u_s is the wave velocity; C_0 and λ are material parameters; R_h is the target plate impedance. This formula demonstrates sound applicability in describing the energy attenuation and reflection-transmission behaviors of detonation waves propagating through composite target plates. It is particularly suitable for analyzing wave propagation characteristics at interfaces between materials with different impedances, providing a quantitative tool for evaluating the protective performance of composite structures.

Through analysis and reference to the research of Xiao Qiangqiang and others, it was found that the incident wave is extensively reflected at the steel-concrete interface, forming reflected tensile waves(Q.Q Xiao et al. 2012). The transmitted compressional waves propagating to the concrete target experience reduced pressure and velocity, resulting in a decrease in the penetration velocity and hole-making capability of the jet on the concrete target. Subsequently, the transmitted wave undergoes further attenuation within the concrete target. When propagating to the third steel target layer, it undergoes additional reflection and transmission, further reducing the jet's penetration velocity and hole-making capability. Therefore, the first and third steel target layers in the designed composite target plate have a greater influence on enhancing the composite target's anti-penetration performance.

5.3 Study on the anti-penetration performance of composite target plates with different thickness ratios

To quantitatively analyze the influence of different steel layer thickness configurations on the anti-penetration performance of the composite target, numerical simulations were conducted by varying the thickness of the upper and middle steel layers respectively. Since a configuration with all three steel layers at 8 mm was required to completely defeat the shaped charge jet, the thickness of either the upper or middle layer was increased starting from 8 mm in increments of 2 mm, while the other two layers remained at the initial thickness of 3 mm.The results indicate that complete protection against the jet was achieved when the first steel layer was increased to 24 mm. Similarly, complete protection was also achieved when the third steel layer reached 22 mm. Compared to the ultimate penetration depth of 660 mm observed in plain concrete, thickening a single steel layer effectively enhanced the protective capacity of the composite target. This study provides a basis for determining the thickness allocation of individual layers in double or triple-layer composite targets with low overall thickness. The damage conditions of the composite targets with different thickness configurations are shown in Figure 16 and Figure 17.

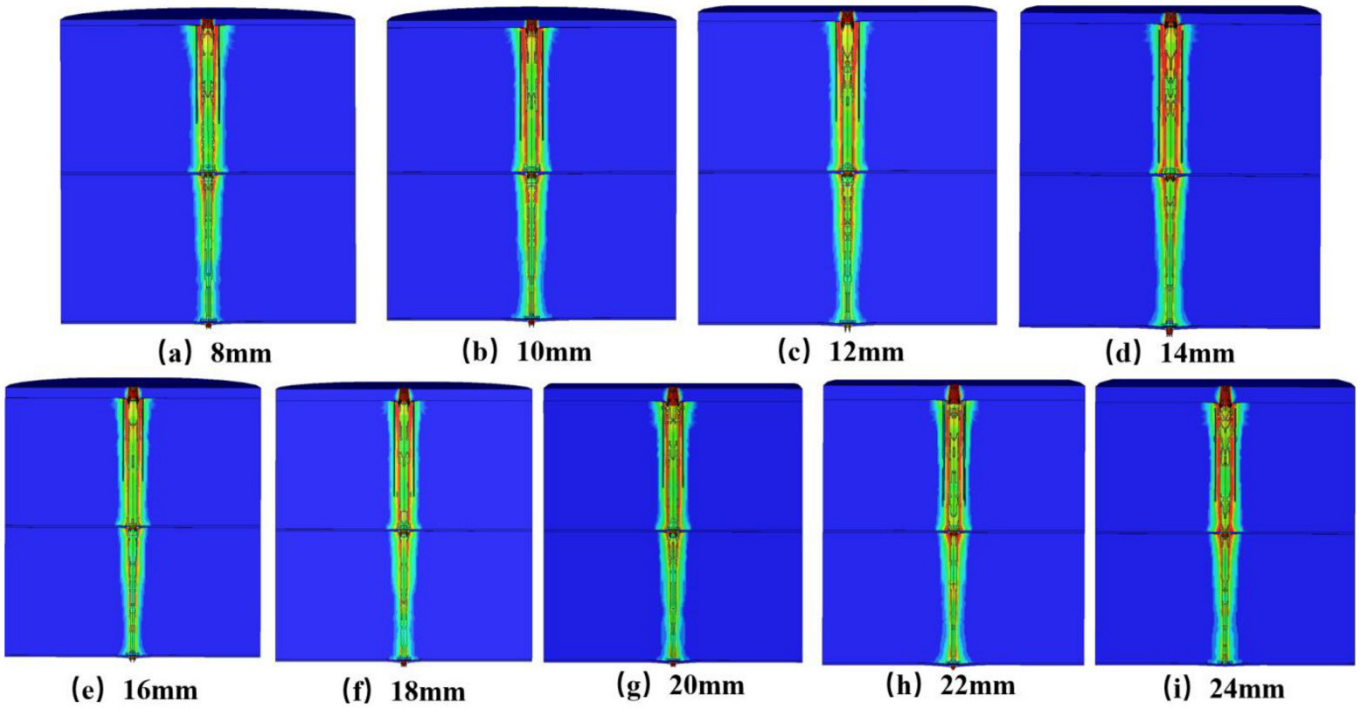

Figure 16. Damage to composite target plates when thickening the upper steel target.

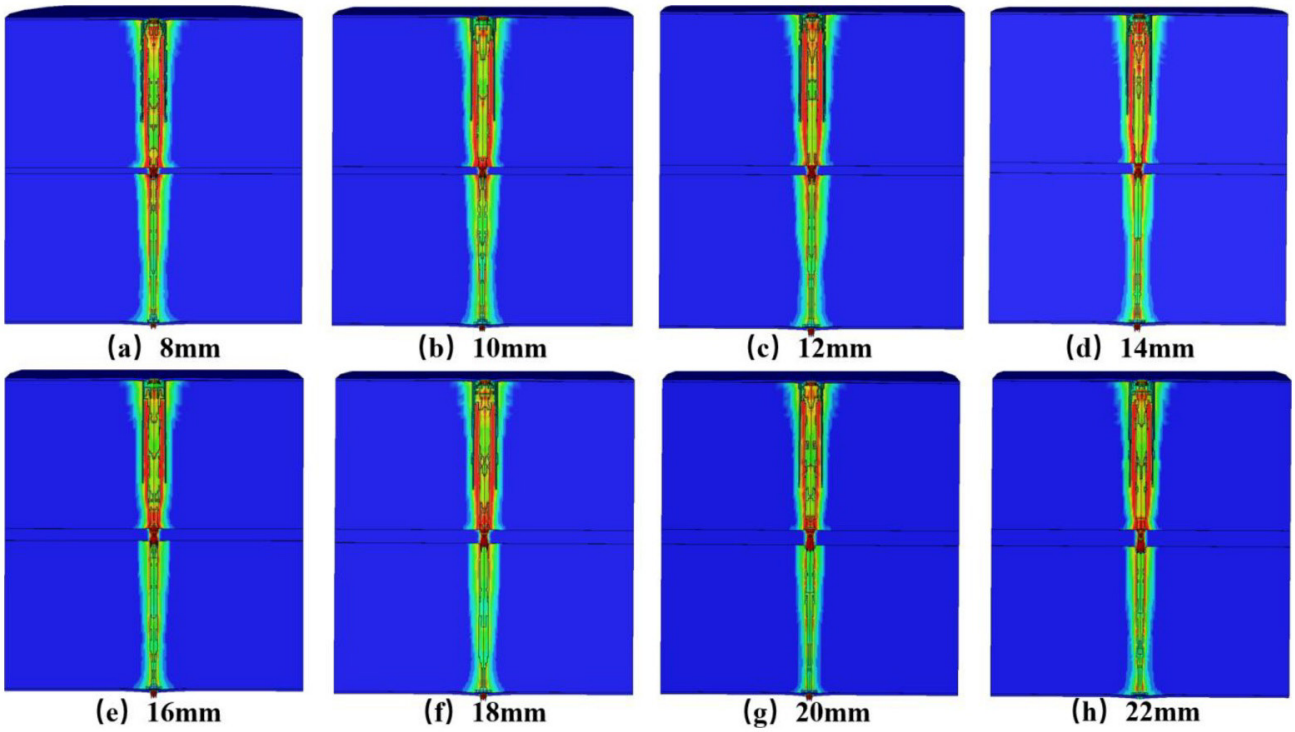

Figure 17. Damage to composite target plates when thickening the middle layer of steel targets.

By comparing the changes in jet penetration velocity at different thicknesses, it can be observed that the jet consumes more energy when penetrating thick steel targets. When the jet penetrates the first layer of the thickened composite target plate, there is a significant velocity decay within the first 200 μs. At this point, the jet's ability to create openings in the concrete target plate significantly decreases. During the subsequent penetration process, the jet's velocity decreases more slowly, and by the time it reaches the fifth layer of the target plate, its velocity is only 683 m/s, making it unable to penetrate the fifth layer of the target plate. When the jet penetrates the third thickened target plate, there is a significant velocity decay between 150 μs and 350 μs. Compared to penetrating the first thickened composite

target plate, the jet has a larger perforation capability on the second concrete target plate and a smaller perforation capability on the fourth concrete target plate. When the jet reaches the fifth layer of the target plate, its velocity is only 753 m/s, which is also insufficient to penetrate the fifth layer of the target plate. The changes in jet velocity when composite target plates of different thickness ratios successfully resist jet penetration are shown in Figure 18.

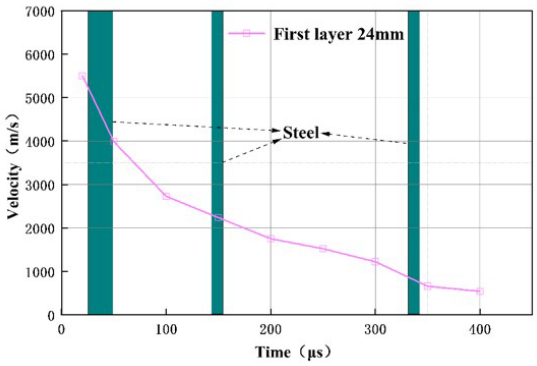

(a) First layer 24mm

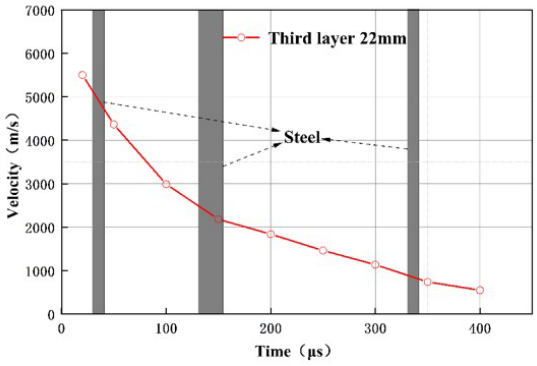

(b) Third layer 22mm

Figure 18. Velocity change of jet not penetrating single-layer thickened composite target plate.

Increasing the thickness of the third layer of steel target in the designed composite target plate can effectively weaken the penetration capability of the jet, but at this point, the damage to the second layer of concrete target is severe, with larger openings. Increasing the thickness of the first layer of steel target can protect the second layer of concrete target while enhancing the composite target plate's resistance to penetration, but the effect on weakening the jet's penetration capability is relatively less pronounced. The changes in the aperture size of the second layer of concrete target plate when composite target plates with different thickness ratios successfully resist jet penetration are shown in Figure 19.

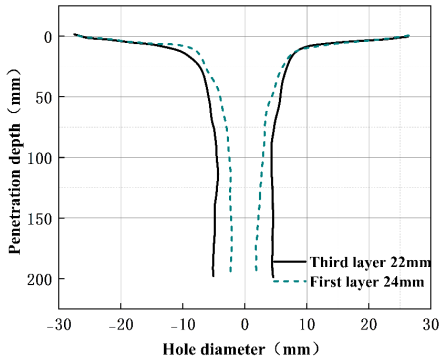

Figure 19. Second layer concrete target hole diameter change.

6 Conclusions

This paper investigates the dynamic response process of concrete targets in composite target plates by conducting static explosion tests on 200-type benchmark projectiles penetrating five-layer composite target plates made of steel and concrete, as well as numerical simulation. It considers the influence of steel plates in composite target plates on improving the penetration resistance of concrete target plates and analyzes the penetration resistance performance of five-layer composite target plates made of steel and concrete. The main conclusions are as follows:

(1) In a five-layer composite target plate consisting of steel-concrete-steel-concrete-steel, the steel target can effectively reduce the destructive power of the shaped charge jet on the concrete target plate, resulting in a 39% reduction in the size of the holes on the concrete target and a 12% reduction in the area of the blast zone. Therefore, in the design of protective structures for civilian or military buildings, the ballistic performance of the protective structure can be enhanced by adding metal plates to the front and back of the concrete plate.

(2) The thickness of the steel target plate in a composite target plate has a significant impact on the composite target plate's penetration resistance. In the designed composite target plate, equivalent calculations revealed that the protective capability of three layers of 8 mm armor steel is equivalent to that of 260 mm C40 concrete, representing a 65% improvement in penetration resistance compared to plain concrete protective structures. Therefore, in the design of composite protective structures, increasing the thickness of the metal plates can reduce costs and the footprint of the building while enhancing concealment and protective performance.

(3) When the composite target plate is below the jet penetration level, stress waves generated during the jet penetration process will undergo reflection and transmission at the interfaces between different media within the composite target plate, thereby influencing the jet penetration process. Taking the steel-concrete interface as an example, under the combined effects of reflected and transmitted waves, the penetration velocity and perforation capability of the jet decrease sharply. Therefore, when designing composite target plates, the protective efficiency can be enhanced by optimizing the acoustic impedance matching relationships between the layers of material.

(4) In a five-layer composite target plate consisting of steel-concrete-steel-concrete-steel, the thickness of the first and third steel layers has a significant impact on the composite target plate's penetration resistance performance, with the third steel layer having a greater influence in the designed structure. Compared to the first layer of steel, which requires a thickness of 24 mm to fully resist penetration by the jet, the third layer only needs a thickness of 22 mm to achieve defense, resulting in a 9.1% improvement in protective performance. Therefore, when designing composite protective structures, it is advisable to consider adjusting the thickness ratios and arrangement of the layers to enhance the structure's penetration resistance.

Author's contributions: Data curation, Conceptualization, Methodology, Writing-Original draft preparation, Software, Visualization, Investigation, Analyses by Bin Chen; Methodology, Visualization, Writing-Reviewing and Editing, Analyses, Funding acquisition by Xudong Zu.

Data availability statement: Research data is available in the body of the article

Editor: Rogério José Marczak

References

Kang, Y. L., Jiang, J. W., Wang, S. Y., et al. Experiment and numerical simulation of shaped charge with different liner materials penetrating multi-layered media [J]. Chinese Journal of High Pressure Physics, 2012, 26(05): 487-493.

Xiao, Q.Q. Research on shaped charge jet penetrating typical soil/concrete composite media target [D]. Nanjing University of Science and Technology, 2012.

Wang, J., Wang, C., Ning, J. G. Research on calculation model of target resistance and numerical simulation for jet penetrating concrete target [J]. Acta Armamentarii, 2008, 29(12): 1409-1416.

Xiao QQ, Huang ZX, Zhu CS, et al. Calculation of depth and crater diameter for the supersonic penetration of shaped charge jet into concrete[J]. Propellants, Explosives, Pyrotechnics, 2013, 38(2): 224-231.

Xiao J, Zhang X, Guo Z, et al. Enhanced Damage Effects of Multi-Layered Concrete Target Produced by Reactive Materials Liner[J]. Propellants, Explosives, Pyrotechnics, 2018, 43(9): 955-961.

Elshenawy T, Li Q M. Influences of target strength and confinement on the penetration depth of an oil well perforator[J]. International Journal of Impact Engineering, 2013, 54: 130-137.

Resnyansky A, Weckert S. Response of an ultra high performance concrete to shaped charge jet[C]//Proceedings of 8th international conference on shock and impact loads on structures, Adelaide. 2009: 529-536.

Xiao QQ, Huang ZX, Jia X, et al. Shaped charge penetrator into soil–concrete double-layered target[J]. International Journal of Impact Engineering, 2017, 109: 302-310.

Zhang Z, Wang L, Silberschmidt V V, et al. SPH-FEM simulation of shaped-charge jet penetration into double hull: A comparison study for steel and SPS[J]. Composite Structures, 2016, 155: 135-144.

Zhu Q, Huang Z, Xiao Q, et al. Theoretical and Experimental Study of Shaped Charge Jet Penetration into High and Ultra-high Strength Concrete Targets[J]. International Journal of Impact Engineering, 2018.

Xu X, Ma T, Ning J. The damage and failure mechanism of the concrete subjected to shaped charge loading[J]. Engineering Failure Analysis, 2017, 82: 741-752.

Liu, Y., Zhang, X. W., Zhang, Q. M. Experimental study on the influence law of shaped charge structure parameters on the penetration and hole-forming behavior in reinforced concrete target [J]. Journal of Ordnance Equipment Engineering, 2025, 46(03): 118-128.

Su, C. H., Wang, Z., Ma, H. B., et al. Dynamic damage characteristics of composite concrete structure subjected to reactive jet [J]. Acta Armamentarii, 2024, 45(S1): 135-146.

HOU JC, WANG CG, Deng DZ, et al.Study on Equivalent Thickness of High Speed Projectile Penetrating into Concrete Target Plate[J].Journal of Ordnance Equipment Engineering,2021,42(02):9-14.

Huang, Z. X., & Zu, X. D. (Eds.). Terminal Effects [M]. Beijing: Science Press, 2014

Du, Z. H., Gao, G. F., & Li, W. B. (Eds.). Impact Dynamics [M]. Beijing: Beijing Institute of Technology Press, 2017.

Gao, Y. H., Liu, T. S., Gu, X. H., et al. Calculation and analysis of shaped charge jet penetrating armor steel [J]. Journal of Projectiles, Rockets, Missiles and Guidance, 2013, 33(01): 84-86+134. DOI:10.15892/j.cnki.djzdxb.2013.01.005.

Wen, W. Z., Yun, S. R., Zhao, H. Y., et al. Numerical simulation of the whole process of shaped charge jet penetrating steel plate [J]. Explosion and Shock Waves, 2001, (02): 126-130.

Wei WL;Chen YQ;Wang ZQ;Li ST;Chen LM;Huang CL.Comparative study on damage effects of penetration and explosion modes on airport runway[J].Construction and Building Materials,2024,411.

Zhang, XW, Xiao, QQ., Huang, ZX., et al. Research on the influence of liner material on jet penetration into high-strength concrete [J]. Journal of Projectiles, Rockets, Missiles and Guidance, 2020, 40(05): 1-4+9. DOI:10.15892/j.cnki.djzdxb.2020.05.001.

Xiao, QQ., Liu, RZ., Feng, CL., et al. Theoretical research on shaped charge jet penetrating soil/concrete composite target [J]. Journal of Vibration and Shock, 2016, 35(17): 102-106. DOI:10.13465/j.cnki.jvs.2016.17.017.

Lu WC, Wu YD, Yu YL, et al. Damage failure and ballistic performance of SiC ceramic-fiber reinforced resin matrix composite armor with different thickness ratios[J]. Acta Materiae Compositae Sinica, 2025, 42(02): 1125-1139. DOI:10.13801/j.cnki.fhclxb.20240508.003.

Liu Z, Lu S, Ji R, et al.Effect of stacking sequence of the hybrid composite armor on ballistic performance and damage mechanism[J].e-Polymers,2025,25(1):20250035-20250035.DOI:10.1515/EPOLY-2025-0035.

Effect of adhesive layer performance on the impact of brittle projectile on B4C ceramic composite armor[J].Acta Mechanica Sinica,2025,42(8):524633-524633.DOI:10.1007/S10409-024-24633-X

HASKELL B N A. The dispersion of source waves in layered media[J]. Bull. Seism. Am, 1953, 43: 17-34.

LAMB H. On the propagation of tremors over the surface of an elastic solid[J]. Phil. Tran. Roy. Soc. A, 1904, 203: 1-42.

Li XB, Lai HH, Gu DS. Reflection-transmission relationships and slip criterion for explosive stress waves obliquely incident on weak structural planes in rock masses[J]. The Chinese Journal of Nonferrous Metals, 1992(01): 9-14.

Wang MY, Qian QH. Attenuation law of explosion waves passing through jointed fracture zones[J]. Chinese Journal of Geotechnical Engineering, 1995, 17(2): 112-119.

Lu DW, Li SZ, Wang YJ. Study on propagation and attenuation law of explosive stress waves[J]. Journal of Chongqing University of Education, 2014, 27(06): 19-21.